Wing Vertical Position Effects on Lift for Supersonic Delta Wing Missiles

A. A. Jenn*
McDonnell Douglas Astronautics Company, St. Louis, Missouri
and
H. F. Nelson†
University of Missouri—Rolla, Rolla, Missouri

The effect of wing vertical position on lift is investigated for supersonic missiles with cylindrical bodies and delta wings. Wing locations above and below the body centerline are considered over a range of Mach number, angle of attack, and aspect ratio. A finite-difference Euler code, SWINT, is used to compute the wing lift. The lift forces are presented in terms of $K_{W(B)}$, which is a measure of wing-body interference due to body upwash. The SWINT $K_{W(B)}$ values for wings located on the missile centerline compare favorably with existing results from theoretical and experimental sources. SWINT results for wings located off the missile centerline indicate that wing lift decreases symmetrically as the wing is moved above or below the centerline. The results are valid for unrolled delta wing-body combinations at moderate-to-high supersonic Mach numbers and at low angles of attack. A simple model based on upwash theory is developed that agrees well with $K_{W(B)}$ predicted by SWINT. Empirical formulas for calculating $K_{W(B)}$ as a function of wing span and vertical position are presented for easy use in preliminary design.

Nomenclature

A_W = planform area of wing formed by joining two fins
$\mathcal{R}$ = aspect ratio of wing formed by joining two fins
B = Mach number parameter, $=\sqrt{M_\infty^2-1}$
C = radial location of bow shock wave
D = body diameter
H = vertical distance between wing and missile centerline
$K_{W(B)}$ = wing-body interference factor due to upwash
K_ϕ = fin-fin interference factor due to sideslip
L_W = lift on wing alone
$L_{W(B)}$ = lift on wing in the presence of body
M = Mach number
$Q_{W(B)}$ = ratio of wing-body interference factors for off-center fins
q = dynamic pressure
R = radius of cylindrical missile body
(r,ϕ,z) = cylindrical missile body coordinates
(r',ϕ') = vertically shifted crossflow coordinates
S = fin span measured from body centerline
V = velocity
Z_W = wing axial location on missile
α = missile angle of attack
α_{eq} = equivalent angle of attack
$(\Delta\alpha_{eq})_v$ = induced change in angle of attack due to vortices
α_F = fin angle of attack
ϕ_F = fin sideslip angle
ϵ = wing semivertex angle
μ = Mach angle, $=\sin^{-1}(1/M_\infty)$

Subscripts

C = crossflow component
N = normal component
r = radial component
W = related to wing
∞ = freestream condition
ϕ = angular component

Introduction

IN missile aerodynamics, mutual interference between neighboring surfaces plays a major role in the performance of a missile configuration. The designer is faced with the challenge of accurately predicting interference effects, usually with time and cost constraints. In the early design stage, when configuration changes are common, correlations based on previously determined theoretical or experimental work can be used effectively to account for the interference between missile components. The purpose of this investigation is to develop a correlation between the wing vertical position on the body and wing lift that is suitable for use in preliminary design.

The effect of wing-body interference has received much attention in literature for missiles with wings located on the missile centerline. Reference 1 characterizes the effect of body upwash on wing lift with an interference factor $K_{W(B)}$, which is defined as

$$K_{W(B)} = \frac{L_{W(B)}}{L_W} \tag{1}$$

Values of $K_{W(B)}$ were determined using linearized potential theory (LPT), slender body theory (SBT), and upwash theory, with each yielding comparable results. It should be noted that these theories are generally valid only for small angles of attack. Additional theoretical studies of wing-body interference using SBT and LPT can be found in Refs. 2-6. Experimental wind-tunnel results for $K_{W(B)}$ are shown in Ref. 7 for a wide variety of missile configurations and flight conditions.

Much less attention has been given to wing-body interference for missile configurations with wings located above or below the body centerline. The effect of wing position on lateral and directional stability derivatives has been experimen-

Received July 11, 1988; presented as Paper 88-4381 at the AIAA Atmospheric Flight Mechanics Conference, Minneapolis, MN, Aug. 15-17, 1988; revision received Dec. 18, 1988.

*Engineer Aeromechanics. Member AIAA.
†Professor of Aerospace Engineering, Thermal Radiative Transfer Group, Department of Mechanical and Aerospace Engineering. Associate Fellow AIAA.

tally investigated for low subsonic flight,[8,9] and a numerical paneling code based on LPT was used in Ref. 10 to determine $K_{W(B)}$ for incompressible flow for a limited number of wing positions and spans.

An important application of $K_{W(B)}$ is in the equivalent angle-of-attack method for predicting lift on missile fins in the presence of a body and other fins. The method models the nonlinear lifting characteristics of missile fins by defining the equivalent angle of attack as

$$\alpha_{eq} = K_{W(B)}\alpha_F + (4/A)K_\phi\alpha_F\beta_F + (\Delta\alpha_{eq})_v \quad (2)$$

where the terms on the right side represent contributions due to body upwash, fin sideslip angle, and vortex interaction, respectively. The equivalent angle-of-attack method is derived and its accuracy is demonstrated in Ref. 11. Extensions of the method to high angles of attack are discussed in Refs. 12 and 13.

Theoretical Background

For a wing located on the centerline of a cylindrical body, LPT, SBT, and upwash theory all predict that the limiting cases of wing-body interference are $K_{W(B)} = 1$ for a wing with no body ($S/R = \infty$) and $K_{W(B)} = 2$ for a small wing on a large body (S/R) = 1.[14] In the first case, as the wing span becomes very large compared to the body radius, the interference between the two components vanishes, and $L_{W(B)}$ approaches L_W, driving $K_{W(B)}$ to unity. The second case can be better understood by considering the crossflow velocity field predicted by LPT.

Two-Dimensional LPT

In cylindrical coordinates, LPT predicts that the crossflow velocity components around a circular body are

$$V_r = -V_C[1 - (R^2/r^2)]\cos\phi$$

$$V_\phi = V_C[1 + (R^2/r^2)]\sin\phi \quad (3)$$

where for small angles of attack $V_C = V_\infty\alpha$.

For a wing located on the missile centerline, the crossflow velocity over the wing can be visualized as shown in Fig. 1. For a very small wing, the flow over the wing is the same as the flow on the body at $\phi = 90$ deg and $r = R$. At this location, the velocity components in Eq. (3) reduce to

$$V_r = 0 \quad \text{and} \quad V_\phi = 2V_C \quad (4)$$

The increase in velocity along the missile body effectively doubles the angle of attack on the small wing compared to the wing-alone case, resulting in twice as much lift and $K_{W(B)} = 2$.

A similar approach can be taken to determine the limiting values of $K_{W(B)}$ for wings located off the missile centerline as a function of H/R. Along the surface of the body,

$$V_r \equiv 0 \quad \text{and} \quad V_\phi = 2V_C\sin\phi \quad (5)$$

In the context of Fig. 2,

$$\theta_W = \sin^{-1}(H/R) \quad (6)$$

and

$$\phi_W = \theta_W + (\pi/2) \quad (7)$$

so that

$$\sin\phi_W = \cos\theta_W \quad (8)$$

and the velocity along the missile body at the wing location becomes

$$V_{\phi_W} = 2V_C\cos\theta_W \quad (9)$$

The wing angle of attack, however, is proportional to the velocity normal to the wing, which is

$$V_{N_W} = 2V_C\cos^2\theta_W \quad (10)$$

and can be rewritten as

$$V_{N_W} = 2V_C(1 - \sin^2\theta_W) \quad (11)$$

Now, using Eq. (6) to get Eq. (11) in terms of H/R,

$$V_{N_W} = 2V_C[1 - (H/R)^2] \quad (12)$$

At this point, $K_{W(B)}$ can be determined as the ratio of the wing angle of attack in the upwash field to the angle of attack of the wing alone in the freestream flow. In terms of crossflow velocities,

$$K_{W(B)} = V_{N_W}/V_C \quad (13)$$

Equations (12) and (13) together give the desired expression for $K_{W(B)}$ as a function of H/R at $S/R = 1$,

$$K_{W(B)}(S/R = 1) = 2[1 - (H/R)^2] \quad (14)$$

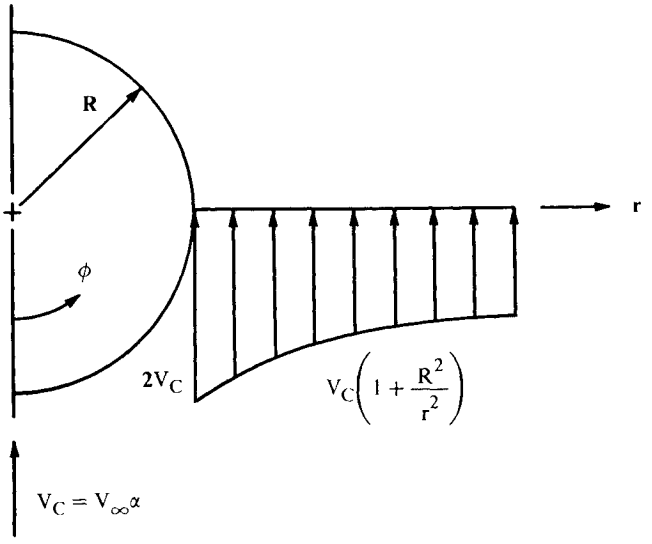

Fig. 1 LPT prediction for crossflow velocity distribution along a wing located on the missile centerline.

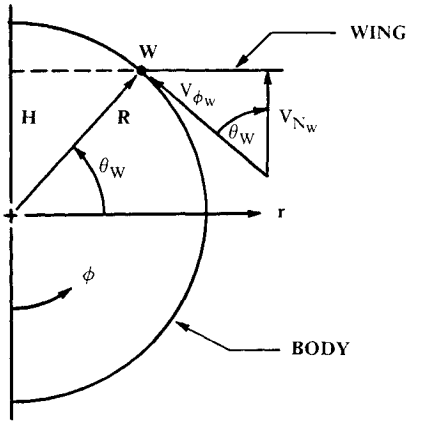

Fig. 2 Crossflow velocity vector diagram used to determine $K_{W(B)}$ ($S/R = 1$) for wings located off the missile centerline.

Panel Upwash Analysis

The local upwash velocity can be used to approximate $K_{W(B)}$ for wings that fall between the limiting values of $1 \leq S/R \leq \infty$. The velocity normal to the wing as a function of spanwise distance along the wing is

$$\frac{V_{N_W}}{V_C} = \left(1 - \frac{R^2}{r^2}\right)\cos^2\phi + \left(1 + \frac{R^2}{r^2}\right)\sin^2\phi \qquad (15)$$

where $r^2 = H^2 + s^2$ and $\phi = \tan^{-1}(H/s) + \pi/2$, with s and r as shown in Fig. 3 for point 2.

Equation (15) gives the upwash velocity at any span position s along the wing leading edge. Strip theory can now be used to determine $K_{W(B)}$ for arbitrary values of S/R. The usual notion of dividing the wing into chordwise strips is modified slightly to include Mach number and aspect ratio effects in the analysis. By considering strips bounded by the right-running Mach lines, as shown in Fig. 3, $K_{W(B)}$ becomes a function of M_∞ and $\mathcal{A}$. Note that $\epsilon > \mu$, indicating that the wing leading edge is supersonic. This modification reduces the wing area influenced by the large upwash velocities near the wing root. As the Mach number becomes very large, the Mach lines become parallel to the chordwise direction and conventional strip theory is obtained. A strip theory formulation using Eq. (15) is

$$K_{W(B)} = \frac{2}{A_W}\sum_{i=1}^{J}\left(\frac{V_{N_W}}{V_C}\right)_i A_i \qquad (16)$$

The application of Eq. (16) is illustrated in Fig. 3 using four panels ($J = 4$) oriented along the Mach lines.

Computational Methodology

Equation (1) shows that two quantities are necessary to calculate $K_{W(B)}$: the wing lift in the presence of the body and the lift on the wing alone. A finite-difference Euler code called SWINT[15] was used to determine wing lift in the presence of the body. SWINT uses an explicit axial marching scheme to solve the conservation equations in a supersonic flow domain bounded by the missile body and the bow shock. SWINT solves the Euler equations in a cylindrical coordinate system (r, ϕ, z) with $r = 0$ along the missile centerline, $\phi = 0$ along the windward side of the missile, and $z = 0$ at the nose of the missile. In this coordinate system, the fins are constrained to lie along constant ϕ planes. The fins are modeled using a thin-fin approximation in which the fin thickness is assumed to be zero; however, the description of the surface slope is retained. SWINT predictions have been shown to agree well with both experimental data and other numerical results for a wide variety of missile configurations and flight conditions.[16,17]

Wing-Alone Lift

Ideally, SWINT would be used to determine L_W in Eq. (1) by determining the lift on a wing composed of two fins joined together at their root chords. SWINT, however, assumes the fins lie entirely within the missile bow shock; therefore, a wing with no body cannot be analyzed. Consequently, LPT was used to determine L_W. For a delta wing with supersonic leading edges,

$$L_W = (4/B)\alpha q_\infty A_W \qquad (17)$$

Equation (17) was used to determine L_W for all cases, since fins with subsonic leading edges were not considered here. A missile with large fins ($S/R = 20$) was analyzed using SWINT to check the SWINT predictions against LPT. As the body becomes small relative to the wing, $L_{W(B)}$ predicted by SWINT asymptotically approaches L_W predicted by LPT. For $S/R > 18$, the two methods give identical results,[18] which shows that the use of Eq. (17) to determine L_W does not compromise the results of the $K_{W(B)}$ analysis.

Missile Geometry

The missile configuration selected for the SWINT runs had a conical nose with a length-to-diameter ratio of 3 and a cylindrical body. The wing was a zero thickness delta wing located at $Z_W/D = 16$ to minimize nose effects on wing lift.[18] The wing aspect ratio was varied from 2.4 to 4.0 and the vertical position was $-0.9 \leq H/R \leq 0.9$. Only one side of the missile was analyzed during each SWINT run. This was possible since the missile configuration was symmetric about a vertical plane passing through the centerline of the missile. Figure 4 shows the missile geometry and some examples of the wing vertical positions.

Coordinate Transformation

In cylindrical coordinates, the cylindrical section of the missile body is easily defined as $r = R$, where R is the radius of the missile. The ϕ planes then extend radially outward from the missile centerline in equally spaced increments from $\phi = 0$ to

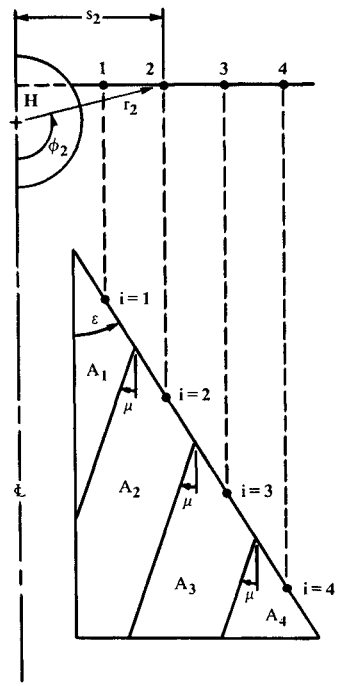

Fig. 3 Paneling geometry used to determine $K_{W(B)}$ ($H/R \neq 0$) from Eq. (16) with $J = 4$.

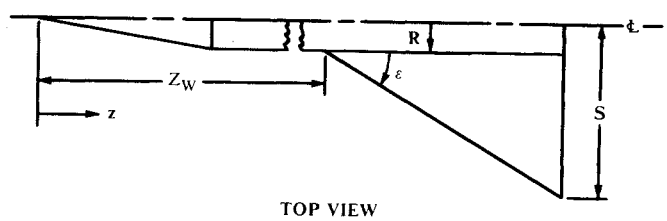

TOP VIEW

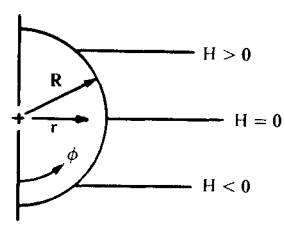

FRONT VIEW

Fig. 4 Missile geometry and nomenclature.

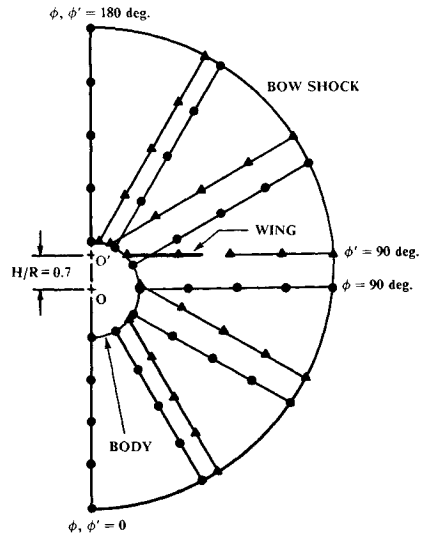

Fig. 5 Unshifted (●) and shifted (▲) coordinate systems used for SWINT analysis.

180 deg. The ϕ increment depends on the number of angular mesh divisions selected for the SWINT run. Seven angular mesh divisions would result in ϕ plane locations of 0, 30, 60, 90, 120, 150, and 180 deg. A wing located at $H/R = 0$ will fall along the $\phi = 90$ deg plane. As the wing is moved vertically away from the missile centerline, the wing will no longer fall along a constant ϕ plane. In order to use SWINT for the analysis, the origin of the coordinate system was shifted by H units from 0 to 0′ as shown in Fig. 5, such that the $\phi = 90$ deg plane again coincided with the wing location.

The method selected to shift the coordinate system takes advantage of a SWINT option that allows the flowfield calculation to be stopped at a given value of z and then restarted with a different mesh density. Stopping the SWINT calculation causes an output file to be saved, which contains the flow properties at each mesh point, shock geometry, and total forces and moments at the value of z where the program was stopped. The coordinate system can then be shifted by redefining the missile geometry and modifying the flowfield output file. This procedure is outlined in the following paragraphs. A detailed description of the coordinate system transformation can be found in Ref. 18.

Missile Geometry Transformation

The missile crossflow geometry in the shifted coordinate system is a circle with the origin located H units above its center as shown in Fig. 5. Letting (r', ϕ') represent the crossflow coordinates in the transformed system, the body radius and required partial derivatives are

$$r' = G_1 + \sqrt{G_3} \tag{18}$$

$$\frac{\partial r'}{\partial \phi'} = -G_2 - \frac{G_1 G_2}{\sqrt{G_3}} \tag{19}$$

$$\frac{\partial^2 r'}{\partial \phi'^2} = -G_1 - \frac{G_1^2 - G_2^2}{\sqrt{G_3}} - \frac{G_1^2 G_2^2}{\sqrt{G_3^3}} \tag{20}$$

where

$$G_1 = H\cos\phi', \quad G_2 = H\sin\phi', \quad \text{and} \quad G_3 = G_1^2 - H^2 + R^2$$

As expected, Eqs. (18-20) reduce to the standard equations for a circle in cylindrical coordinates when $H = 0$. Note that the wing planform definition is also affected by the shifted coordinate system. As the magnitude of H is increased, the distance from the origin 0′ to the wing tips decreases as shown in Eq. (21), as

$$S' = \sqrt{R^2 - H^2} + (z - Z_W)\tan\epsilon \tag{21}$$

Bow Shock and Flowfield Transformation

As the coordinate system is shifted, the coordinates of the bow shock and the finite-difference mesh points change as functions of H. The locations of the new bow shock grid points are determined by projecting the original shock point locations into the new coordinate system using the following equations:

$$r' = [(r\sin\phi)^2 + (r\cos\phi + H)^2]^{1/2} \tag{22}$$

$$\phi' = \tan^{-1}\frac{r\sin\phi}{r\cos\phi + H} \tag{23}$$

and then linearly interpolating on ϕ' to find the location of the bow shock C'. The remaining flowfield mesh points are then located along each ϕ' plane in evenly spaced r' increments between the missile body and the bow shock. Figure 5 shows the original and new mesh point locations for a coordinate shift of $H/R = 0.7$. The only remaining task is to determine the flowfield properties at the new mesh points. This is done by projecting the old mesh point locations into the shifted coordinate system using Eqs. (22) and (23) and then using bilinear interpolation to determine the flowfield properties at each mesh point.

A FORTRAN program was written to carry out the coordinate transformation described above and to change the flowfield mesh density if desired. Thus, it was possible to use SWINT to generate a flowfield output file for each flight condition at a crossflow plane just ahead of the wing location. The computer program was then used to generate a new flowfield output file with the coordinate system shifted to the desired value of H/R. SWINT was then started with the new flowfield data file for analysis of the winged section of the missile. This also allowed verification of the coordinate transformation procedure. The crossflow flowfields at $z/D = 20$ on a body with no wing were determined using SWINT with shifted coordinate systems located at $H/R = \pm 0.9$. The flowfields were compared with a flowfield from SWINT in which no coordinate transformation was used. In each case, the flowfield properties were nearly identical, indicating that the coordinate transformation procedure was correct.

Results and Discussion

All SWINT predictions were made with a uniformly distributed finite-difference mesh. Twenty radial mesh divisions and ten angular mesh divisions (20 × 10 mesh) were used for $z/D < 5$. This was increased to a 40 × 20 mesh for $z/D < 10$ and a 60 × 30 mesh for $z/D < 15$. At $z/D = 15$, the coordinate system was shifted to the desired value of H/R and the mesh size was increased to 72 × 37 for analysis of the winged section of the missile. After each axial step along the wing was completed, z and $L_{W(B)}$ were saved so that $K_{W(B)}$ and S/R could be calculated using Eqs. (10) and (24), respectively,

$$\frac{S}{R} = \frac{(z - Z_W)}{R}\tan\epsilon + 1 \tag{24}$$

Strictly, Eq. (21) should be used to determine S/R for wings located off the missile centerline. This implies, however, that two identical fins located at different vertical positions would have different values of S/R. For purposes of data comparison, this was not practical. Consequently, all values of S/R presented hereafter were determined with Eq. (24) as if the wing was located on the missile centerline. This implies that S is computed as the sum of the body radius and the exposed fin span. Therefore, S/R always varies from one to infinity regardless of the fin vertical position.

SWINT runs were made at six flight conditions with three wing planforms to determine the effects of M_∞, α, and $\mathcal{R}$ on $K_{W(B)}$ as shown in Table 1. Mach number was varied between 2.5 and 4.0 in increments of 0.5 at $\alpha = 3$ deg and $\mathcal{R} = 3.2$. Angle of attack was varied between 2 and 4 deg in increments of 1 deg at $M_\infty = 3.0$ and $\mathcal{R} = 3.2$. Aspect ratio was varied between 2.4 and 4.0 in increments of 0.8 at $M_\infty = 3.0$ and $\alpha = 3$ deg. For each combination of M_∞, α, and $\mathcal{R}$, wing locations of $H/R = 0$, ± 0.5, ± 0.7, and ± 0.9 were used. In each case, $K_{W(B)}$ was determined for $1 \leq S/R \leq 6$, although the values of $K_{W(B)}$ at $S/R \leq 1.3$ were generally inaccurate due to an inadequate number of mesh points located on the small fins.

SWINT Results and Comparisons

Figure 6 compares SWINT results for $K_{W(B)}$ with results from the various theories presented in Ref. 1 for wings located on the missile centerline. The SWINT predictions are slightly larger than LPT and SBT and somewhat smaller than the upwash theory implemented with chordwise strips. In all cases, the maximum difference between the four methods was small. A value of $K_{W(B)}$ from SWINT was also compared to an experimental value reported in Ref. 7. A SWINT run made at $M_\infty = 3.5$, $\alpha = 3$ deg, $\mathcal{R} = 2.0$, $H/R = 0$, and $S/R = 2$ gave $K_{W(B)} = 1.58$. The $K_{W(B)}$ value from Ref. 7 at the same conditions was 1.53, a difference of only 3.3%.

Effect of Wing Position

The SWINT results for $K_{W(B)}$ at $M_\infty = 3.0$, $\alpha = 3$ deg, and $\mathcal{R} = 3.2$ are shown in Fig. 7 for seven values of H/R. The solid lines are for positive values of H/R and the dashed lines are for negative H/R values. At small values of S/R, $K_{W(B)}$ decreases as the wing is moved up or down from the missile centerline. As S/R is increased, the effect of wing position on $K_{W(B)}$ decreases and the curves all approach the limiting value of $K_{W(B)} = 1$. Two significant trends are apparent in Fig. 7: 1) $K_{W(B)}$ is sensitive only to the magnitude of the wing shift and not to the direction; and 2) at small values of S/R, the $K_{W(B)}$ curves all approach the limiting values predicted in Eq. (14), as indicated by the solid circles at $S/R = 1$. These two trends support the assumption that $K_{W(B)}$ is governed by the crossflow velocity distribution for wings located on or off the missile centerline.

The $K_{W(B)}$ results at the other flight conditions and aspect ratios are available in Ref. 18. The additional results indicate that $K_{W(B)}$ is not a function of M_∞, α, or $\mathcal{R}$ for the ranges of the parameters presented in Table 1. In all cases, the $K_{W(B)}$ results were nearly identical to the values shown in Fig. 7.

Comparison of SWINT and Upwash Theory

SWINT results for lift on wings located off the missile centerline were compared to data from the upwash formulation shown in Eq. (16). Figure 8 shows $K_{W(B)}$ values from SWINT and Eq. (16) for $H/R = 0$, ± 0.5, ± 0.7, and ± 0.9. Note that the SWINT results have been extended to their limiting values from Eq. (14) at $S/R = 1$, as discussed in the next section. Good agreement between the two methods is evident, especially as the magnitude of H/R increases. This is significant, since Eq. (16) is Mach number independent, with the exception of using the Mach angle to determine the panel geometry in the strip theory formulation.

Preliminary Design Formulation

The $K_{W(B)}$ values in Fig. 7 were modified slightly for use in preliminary design. The small differences between the two curves at each value of H/R were removed by averaging the $K_{W(B)}$ values obtained at $+H/R$ and $-H/R$, resulting in a

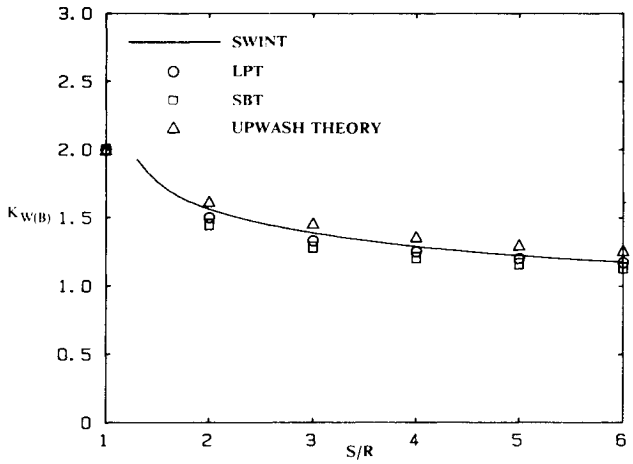

Fig. 6 Comparison of $K_{W(B)}$ ($H/R = 0$) from SWINT at $M_\infty = 3.0$, $\alpha = 3$ deg, and $\mathcal{R} = 3.2$ to various analytical solutions.

Table 1 Flight conditions and aspect ratios used to determine $K_{W(B)}$

M_∞	α	$\mathcal{R}$	H/R
2.5	3	3.2	0, ± (0.5, 0.7, 0.9)
3.0	2	3.2	0, ± (0.5, 0.7, 0.9)
3.0	3	2.4	0, ± (0.5, 0.7, 0.9)
3.0	3	3.2	0, ± (0.1, 0.2, ..., 0.9)
3.0	3	4.0	0, ± (0.5, 0.7, 0.9)
3.0	4	3.2	0, ± (0.5, 0.7, 0.9)
3.5	3	3.2	0, ± (0.5, 0.7, 0.9)
4.0	3	3.2	0, ± (0.5, 0.7, 0.9)

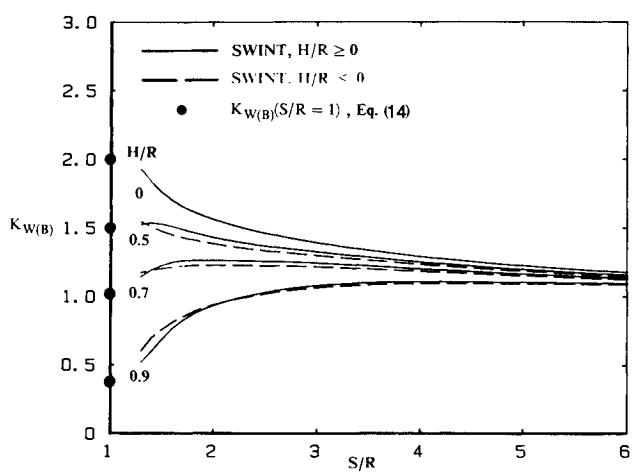

Fig. 7 SWINT $K_{W(B)}$ vs wing span and wing vertical location at $M_\infty = 3.0$, $\alpha = 3$ deg, and $\mathcal{R} = 3.2$.

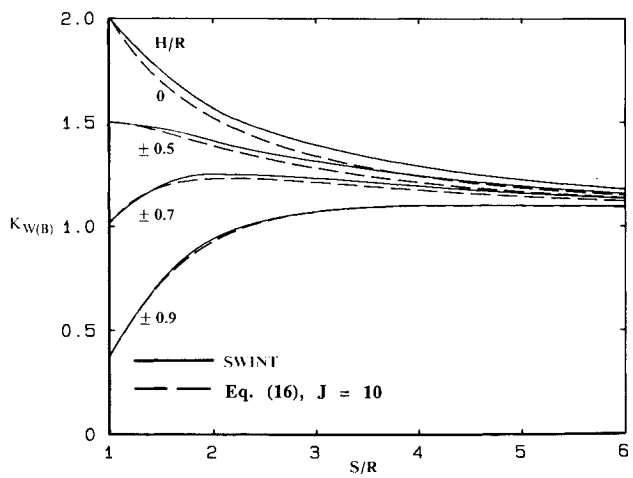

Fig. 8 Comparison of SWINT $K_{W(B)}$ and upwash theory paneling method [Eq. (16)] at $M_\infty = 3.0$, $\alpha = 3$ deg, and $\mathcal{R} = 3.2$.

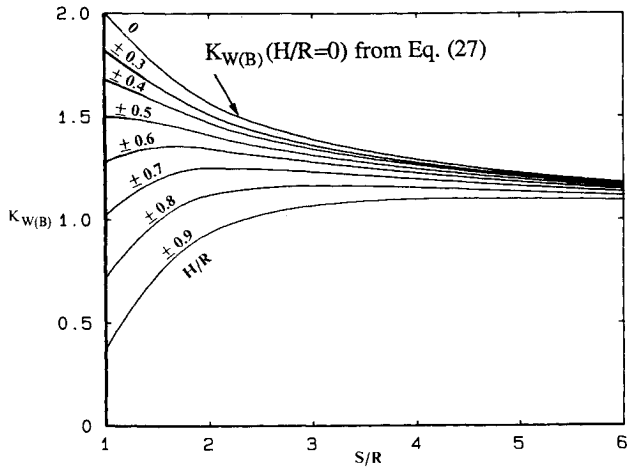

Fig. 9 SWINT $K_{W(B)}$ results modified for use in preliminary design.

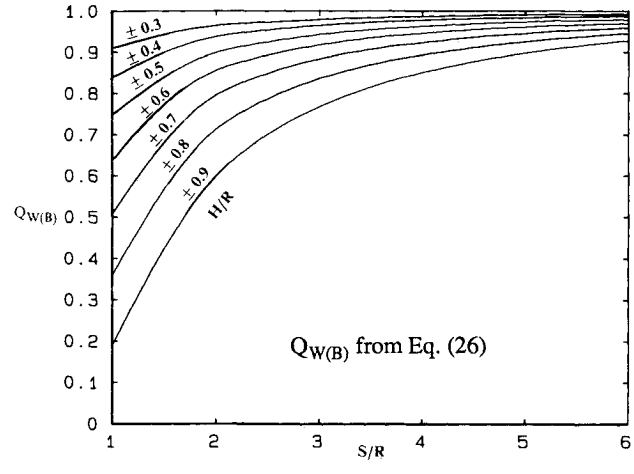

Fig. 10 SWINT $Q_{W(B)}$ results for use in preliminary design.

single curve valid for $\pm H/R$. Also, the $K_{W(B)}$ results for $1 \leq S/R \leq 2$ were replaced by a second-order polynomial. The conditions placed on the polynomial were that the magnitude and slope must match the averaged SWINT results at $S/R = 2$ and the magnitude at $S/R = 1$ must match that given by Eq. (14). The $K_{W(B)}$ values obtained following these modifications are shown in Fig. 9 for $H/R = 0$ to ± 0.9 in increments of ± 0.1. Results at $H/R = \pm 0.1$ and ± 0.2 are not shown to preserve clarity. The polynomial fit was necessary because $K_{W(B)}$ from SWINT was inaccurate for $S/R < 1.3$. It essentially extended the $K_{W(B)}$ curves to their potential flow values at $S/R = 1$, without affecting the magnitude of the SWINT calculation.

The effect of wing position on wing-body interference is presented in a different form in Fig. 10. Here, as Ref. 10 suggests, $Q_{W(B)}$ is defined as the ratio of the lift on the wing located off the missile centerline to the lift of a wing located on the centerline such that

$$Q_{W(B)} = \frac{K_{W(B)}(H/R \neq 0)}{K_{W(B)}(H/R = 0)} \tag{25}$$

$Q_{W(B)}$ can be used with $K_{W(B)}(H/R = 0)$ data obtained from sources such as wind-tunnel tests or Fig. 9 to make preliminary design predictions for the lift on wings located above or below the missile centerline. To further simplify this task, an empirical fit of the curves in Fig. 10 was developed as a function of H/R and S/R, as

$$Q_{W(B)} = 1 - \frac{(H/R)^2}{(0.7\sqrt{1 - H/R} + 0.6)^{2/\sqrt{S/R}}\,(S/R)\ln(S/R) + 1} \tag{26}$$

This matches the curves in Fig. 10 to within 1%. In addition, the mathematical nature of Eq. (26) allows extrapolation beyond $S/R = 6$ and $H/R = 0.9$, while preserving the correct limits as $S/R \to \infty$ and $H/R \to 1$.

An additional empirical curve fit of the $K_{W(B)}(H/R = 0)$ results from Fig. 9 is

$$K_{W(B)} = 1 + \frac{1}{0.43[1 + 0.29(S/R - 0.8)^{-(S/R)/2}]\,(S/R)\ln(S/R) + 1} \tag{27}$$

Again, the equation is accurate to within 1% and can be used for large values of S/R. Equations (25-27) together can be used to reproduce accurately all of the SWINT results for $K_{W(B)}$ obtained in this research.

Conclusions and Recommendations

A finite-difference Euler code has been used to determine the effect of wing vertical position on wing lift for supersonic delta wing missiles at small angles of attack. Values of $K_{W(B)}$ were determined for wing positions of $-0.9 \leq H/R \leq 0.9$ and wing spans of $1 \leq S/R \leq 6$. $K_{W(B)}$ was found to decrease symmetrically as the wing was moved above or below the missile centerline. The magnitude of $K_{W(B)}$ approached one for all wing locations as the wing span became large compared to the body radius. The effects of M_∞, α, and AR on $K_{W(B)}$ were investigated and found to be small over the ranges considered. SWINT results for $K_{W(B)}$ at $H/R = 0$ were shown to be in good agreement with results from LPT, SBT, upwash theory, and experimental wind-tunnel data. At small and large values of S/R, $K_{W(B)}$ from SWINT was shown to agree with the limiting values of $K_{W(B)}$ predicted with two-dimensional LPT. A strip theory model based on upwash theory also agreed well with SWINT results over the entire range of S/R. Finally, two empirical equations were presented that correlate the SWINT results for wing-body interference over the entire ranges of H/R and S/R. These equations are ideally suited for preliminary design prediction of $K_{W(B)}$ or for use in correcting $K_{W(B)}(H/R = 0)$ data to account for the effects of changes in the wing vertical position.

Future research on $K_{W(B)}$ is needed to determine the effect of wing position on wing lift for missiles operating at higher angles of attack and Mach numbers where vortices, crossflow shock waves, and viscous effects must be considered. The symmetry of $K_{W(B)}$ with high/low-wing vertical positions is not expected to be valid when nonlinear body-induced effects become important. In addition, future work should include evaluating the wing-on-body lift carryover $K_{W(B)}$ and the effect of different wing planform shapes using Euler approaches. The effect of off-midplane fins on K_ϕ also needs to be investigated. At lower angles of attack and Mach numbers, the strip model based on the upwash theory discussed herein could be further developed to account for various wing planforms and body shapes at subsonic, transonic, and supersonic speeds.

Acknowledgments

This work was supported by McDonnell Douglas Astronautics Company, St. Louis, through the Independent Research and Development program, monitored by John E. Williams. Additional funds were provided by the Missouri Research Assistance Act.

References

[1]Pitts, W. C., Nielsen, J. N., and Kaattari, G. E., "Lift and Center of Pressure of Wing-Body-Tail Combinations at Subsonic, Transonic, and Supersonic Speeds," NACA Rept. 1307, 1957.

[2]Nielsen, J. N., *Missile Aerodynamics,* McGraw-Hill, New York, 1960.

[3]Nielsen, J. N. and Pitts, W. C., "Wing-Body Interference at Supersonic Speeds with an Application to Combinations with Rectangular Wings," NACA TN-2677, 1952.

[4]Lomax, H. and Byrd, P. F., "Theoretical Aerodynamic Characteristics of a Family of Slender Wing-Tail-Body Combinations," NACA TN-2554, 1951.

[5]Ferrari, C., "Interference Between Wing and Body at Supersonic Speeds—Theory and Numerical Application," *Journal of the Aeronautical Sciences,* Vol. 15, June 1948, pp. 317–336.

[6]Morikawa, G., "Supersonic Wing-Body Lift," *Journal of the Aeronautical Sciences,* Vol. 18, April 1951, pp. 217–228.

[7]Nielsen, J. N., "Supersonic Wing-Body Interference at High Angles of Attack with Emphasis on Low Aspect Ratios," AIAA Paper 86-0568, 1986.

[8]Goodman, A. and Thomas, D. F., Jr., "Effects of Wing Position and Fuselage Size on the Low-Speed Static and Rolling Stability Characteristics of a Delta Wing Model," NACA Rept. 1224, 1955.

[9]Jaquet, B. M. and Fletcher, H. S., "Experimental Steady State Yawing Derivatives of a 60 Deg. Delta-Wing Model as Affected by Changes in Vertical Position of the Wing and in Ratio of Fuselage Diameter to Wing Span," NACA TN-3843, 1956.

[10]Sutcliffe, S. G. and Hunt, B., "The Prediction of Wing-Body Interference Using the B. Ae. Mk. II Panel Program and Comparison with Data-Sheet Results," British Aerospace Aircraft Group, Warton, England, UK, Rept. Ae/A/673, Jan. 1981.

[11]Hemsch, M. J. and Nielsen, J. N., "Equivalent Angle-of-Attack Method for Estimating Nonlinear Aerodynamics of Missile Fins," *Journal of Spacecraft and Rockets,* Vol. 20, July–Aug. 1983, pp. 356–362.

[12]Hemsch, M. J. and Nielsen, J. N., "Extension of Equivalent Angle-of-Attack Method for Nonlinear Flowfields," *Journal of Spacecraft and Rockets,* Vol. 22, No. 3, May–June 1985, pp. 304–308.

[13]Stoy, S. L. and Vukelich, S. R., "Extension of the Equivalent Angle of Attack Prediction Method," AIAA Paper 84-0311, 1984.

[14]Nielsen, J. N., "Nonlinearities in Missile Aerodynamics," AIAA Paper 78-20, 1978.

[15]Wardlaw, A. B., Hackerman, L. B., and Baltakis, F. P., "An Inviscid Computational Method for Supersonic Missile Type Bodies. Program Description and Users Guide," Naval Surface Weapons Center, TR 81-459, Dec. 1981.

[16]Wardlaw, A. B., Baltakis, F. P., and Solomon, J. M., "Supersonic Inviscid Flowfield Computations of Missile Type Bodies," *AIAA Journal,* Vol. 19, July 1981, pp. 899–906.

[17]Priolo, F. J. and Wardlaw, A. B., "A Comparison of Inviscid Computational Methods for Supersonic Tactical Missiles," AIAA Paper 87-0113, 1987.

[18]Jenn, A. A., "Numerical Determination of Missile Aerodynamic Interference Factors," M. S. Thesis, Dept. of Mechanical and Aerospace Engineering, Univ. of Missouri, Rolla, Dec. 1987.